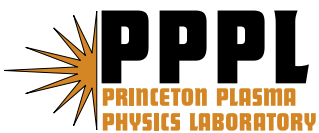


**Full-wave Simulations of ICRF Heating in Toroidal Plasma
with Non-Maxwellian Distribution Functions in the FLR Limit**

E.J. Valeo, C.K. Phillips, H. Okuda, J.C. Wright,
P.T. Bonoli, L.A. Berry, and the RF SciDAC Team

July 2007



Princeton Plasma Physics Laboratory

Report Disclaimers

Full Legal Disclaimer

This report was prepared as an account of work sponsored by an agency of the United States Government. Neither the United States Government nor any agency thereof, nor any of their employees, nor any of their contractors, subcontractors or their employees, makes any warranty, express or implied, or assumes any legal liability or responsibility for the accuracy, completeness, or any third party's use or the results of such use of any information, apparatus, product, or process disclosed, or represents that its use would not infringe privately owned rights. Reference herein to any specific commercial product, process, or service by trade name, trademark, manufacturer, or otherwise, does not necessarily constitute or imply its endorsement, recommendation, or favoring by the United States Government or any agency thereof or its contractors or subcontractors. The views and opinions of authors expressed herein do not necessarily state or reflect those of the United States Government or any agency thereof.

Trademark Disclaimer

Reference herein to any specific commercial product, process, or service by trade name, trademark, manufacturer, or otherwise, does not necessarily constitute or imply its endorsement, recommendation, or favoring by the United States Government or any agency thereof or its contractors or subcontractors.

PPPL Report Availability

Princeton Plasma Physics Laboratory:

<http://www.pppl.gov/techreports.cfm>

Office of Scientific and Technical Information (OSTI):

<http://www.osti.gov/bridge>

Related Links:

[U.S. Department of Energy](#)

[Office of Scientific and Technical Information](#)

[Fusion Links](#)

Full-wave Simulations of ICRF heating in toroidal plasma with non-Maxwellian distribution functions in the FLR limit

E. J. Valeo, C. K. Phillips, and H. Okuda

Plasma Physics Laboratory,

Princeton University

Princeton, NJ

J. C. Wright and P. T. Bonoli

Plasma Science Fusion Center, MIT

Cambridge, MA

L. A. Berry

Oak Ridge National Laboratory

Oak Ridge, TN

RF SciDAC Team

At the power levels required for significant heating and current drive in magnetically-confined toroidal plasma, modification of the particle distribution function from a Maxwellian shape is likely [T. H. Stix, *Nucl. Fusion*, 15:737 1975], with consequent changes in wave propagation and in the location and amount of absorption. In order to study these effects computationally, the finite-Larmor-radius, full-wave, hot-plasma toroidal simulation code, TORIC [M. Brambilla. *Plasma Phys. Controlled Fusion*, 41:1, 1999.], has been extended to allow the prescription of arbitrary velocity distributions of the form $f(v_{\parallel}, v_{\perp}, \psi, \theta)$. For H minority heating of a D(H) plasma with anisotropic Maxwellian H distributions, the fractional H absorption varies significantly with changes in parallel temperature but is essentially independent of perpendicular temperature.

I. INTRODUCTION

The injection of waves in the ion cyclotron frequency range is a well-established method of heating and driving current in magnetically confined toroidal plasma. A straightforward estimate suggests that, at rf power levels which are sufficiently high that finite enhancements in temperature or current are achieved, the ion velocity distribution functions are expected to be significantly modified from a thermal, Maxwellian shape[1]. Since the absorption of energy and momentum are overwhelmingly through collisionless wave-particle interactions, local in velocity space, these distribution function modifications will, generally, result in finite changes in the amount and spatial location of absorption. Inclusion of these modifications, ultimately computed self-consistently together with the wave fields, is required to more faithfully model experimental results and to more accurately design future devices.

There has been substantial progress recently to address these considerations. The one-spatial-dimensional (1D) all-order quasi-local code METS[3] has been extended to handle arbitrary gyrotropic distribution functions and has been applied to simulate ion cyclotron resonance heating (ICRH) in magnetic fusion plasmas in which neutral beam injection is also applied[4]. More recently, the all-orders (in Larmor radius to wavelength) global-wave solver AORSA[5, 6] has been coupled to the CQL3D Fokker-Planck code[7]. The combination has been iteratively solved to self-consistently compute wave-fields and ion distribution functions[8].

Here, we describe the extension of the TORIC-2D finite Larmor radius code[2, 9] to include non-Maxwellian distribution functions. TORIC differs from the all-orders codes in that it makes use of the assumption that the ion Larmor radius ρ_i is small-but-finite compared to the scale of wave field variation perpendicular to the local magnetic field direction, $\hat{\mathbf{b}}$, *ie.*, $\rho_i |\hat{\mathbf{b}} \wedge \nabla A / A| \ll 1$, for any field component A . This approximation greatly reduces computational burden while still accurately reproducing results obtained from the more general codes when the small-Larmor-radius approximation is verified *a posteriori*.

The code is described briefly in Section II, where the extensions are presented in detail. The numerical implementation is presented in Section III. Results of trial applications are presented in Section IV, followed by a discussion in Section V.

II. CODE DESCRIPTION

The TORIC code solves the vector wave equation

$$\nabla \wedge \nabla \wedge \mathbf{E} = \frac{\omega^2}{c^2} [\mathbf{E} + \frac{4\pi i}{\omega} (\mathbf{J}^P + \mathbf{J}^A)] \quad (1)$$

for the vector electric field \mathbf{E} . The undriven plasma is assumed time independent and toroidally symmetric. Therefore, the response to a prescribed antenna current density $\mathbf{J}^A(\mathbf{x}_p, \phi, t)$ as a function of poloidal position \mathbf{x}_p , toroidal angle ϕ , and time t , can be obtained by summation of responses to each Fourier component $\mathbf{J}^A(\mathbf{x}_p, n, \omega) \exp i(n\phi - \omega t)$ with frequency ω and toroidal mode number n . The plasma current density \mathbf{J}^P ,

$$\mathbf{J}^P \equiv \sum_j q_j \int d\mathbf{v} \mathbf{v} f_j(\mathbf{x}, \mathbf{v}, \omega) \quad (2)$$

requires the solution for the particle distribution functions $f_j(\mathbf{x}, \mathbf{v}, \omega)$, for each species j , which is computed by solving the linearized Vlasov equation with several assumptions: the particle gyro-radii are small compared to the scale of field variation perpendicular to the local magnetic field direction, $\mathbf{b} \equiv \mathbf{B}/|\mathbf{B}|$; the effects of drifts across the magnetic flux surfaces are negligible; multiple resonant wave-particle interactions are uncorrelated. The small-Larmor-radius approximation reduces the response to cross-field variations of \mathbf{E} from an integral to a differential form. Spatial dependence is further decomposed into variation within and across poloidal flux surfaces, $\psi(\mathbf{x}) = \text{const}$. Fourier decomposition of variation within surfaces,

$$A(r, z) = \sum_m A_m(\psi) e^{im\theta} \quad (3)$$

and projection of the wave equation onto test functions $\mathbf{F}(\psi)$ with compact support transforms the system into a dense block (in m) - tridiagonal (in ψ) system which is soluble using standard numerical methods. By virtue of this decomposition, the local parallel component of the wavevector is explicitly represented as

$$k_{\parallel}(\theta, \psi) \equiv \mathbf{k} \cdot \mathbf{b} = (m\nabla\theta + n\nabla\phi) \cdot \mathbf{b} \quad (4)$$

This representation facilitates the required computation of the elements of the local susceptibility tensor χ_j relating the current in species j , \mathbf{J}_j^P to the driving electric field

$$\mathbf{J}_j^P = -\frac{i\omega}{4\pi} \chi_j \cdot \mathbf{E} \quad (5)$$

In a local coordinate (Stix[10]) frame $(\hat{\mathbf{x}}, \hat{\mathbf{y}}, \hat{\mathbf{z}})$, with $\hat{\mathbf{z}} = \mathbf{b}$, $\mathbf{k} \cdot \hat{\mathbf{y}} = 0$, to second order in $k_{\perp}v_{\perp}/\Omega_c$, and for velocity distribution functions of the form

$$f_j(\mathbf{v}) = f_j(v_{\perp}, v_{\parallel}) \quad (6)$$

these components can be written as[11]

$$\begin{aligned} \chi_{xx} &= \frac{\omega_p^2}{\omega} \left\{ \frac{1}{2}(A_{1,0} + A_{-1,0}) - \frac{\lambda}{2}(A_{1,1} + A_{-1,1}) + \frac{\lambda}{2}(A_{2,1} + A_{-2,1}) \right\}, \\ \chi_{xy} = -\chi_{yx} &= i \frac{\omega_p^2}{\omega} \left\{ \frac{1}{2}(A_{1,0} - A_{-1,0}) - \lambda(A_{1,1} - A_{-1,1}) + \frac{\lambda}{2}(A_{2,1} - A_{-2,1}) \right\}, \\ \chi_{xz} = +\chi_{zx} &= \frac{\omega_p^2}{\omega} \left(\frac{1}{2} \frac{k_{\perp}}{\Omega} \right) \left\{ (B_{1,0} + B_{-1,0}) - \lambda(B_{1,1} + B_{-1,1}) + \frac{\lambda}{2}(B_{2,1} + B_{-2,1}) \right\}, \\ \chi_{yy} &= \frac{\omega_p^2}{\omega} \left\{ 2\lambda A_{0,1} + \frac{1}{2}(A_{1,0} + A_{-1,0}) - \frac{3\lambda}{2}(A_{1,1} + A_{-1,1}) \right. \\ &\quad \left. + \frac{\lambda}{2}(A_{2,1} + A_{-2,1}) \right\}, \\ \chi_{yz} = -\chi_{zy} &= i \frac{\omega_p^2}{\omega} \left(\frac{k_{\perp}}{\Omega} \right) \left\{ B_{0,0} - \lambda B_{0,1} - \frac{1}{2}(B_{1,0} + B_{-1,0}) - \lambda(B_{1,1} + B_{-1,1}) \right. \\ &\quad \left. - \frac{\lambda}{4}(B_{2,1} + B_{-2,1}) \right\}, \end{aligned} \quad (7)$$

and

$$\begin{aligned} \chi_{zz} &= \frac{2\omega_p^2}{k_{\parallel}w_{\perp}^2} \left[(1 - \lambda)B_{0,0} + \int_{-\infty}^{\infty} dv_{\parallel} \int_0^{\infty} dv_{\perp} v_{\perp} \frac{v_{\parallel}}{\omega} f_0(v_{\parallel}, v_{\perp}) \right] \\ &\quad + \frac{\lambda \omega_p^2}{2 \omega} \left[2 \frac{(\omega - \Omega)}{k_{\parallel}w_{\perp}^2} B_{+1,0} + 2 \frac{(\omega + \Omega)}{k_{\parallel}w_{\perp}^2} B_{-1,0} \right], \end{aligned} \quad (8)$$

where

$$\lambda \equiv \frac{1}{2} \left(\frac{k_{\perp}w_{\perp}}{\Omega} \right)^2, \quad (9)$$

with

$$w_{\perp}^2 \equiv 2\pi \int_{-\infty}^{\infty} dv_{\parallel} \int_0^{\infty} dv_{\perp} v_{\perp} v_{\perp}^2 f(v_{\perp}, v_{\parallel}). \quad (10)$$

Here, the coefficients

$$\left\{ \begin{array}{c} A_{n,j} \\ B_{n,j} \end{array} \right\} \equiv 2\pi \int_{-\infty}^{\infty} dv_{\parallel} \left\{ \frac{1}{v_{\parallel}} \right\} \frac{1}{\omega - k_{\parallel}v_{\parallel} - n\Omega} \int_0^{\infty} dv_{\perp} v_{\perp} H_j(v_{\parallel}, v_{\perp}) \quad (11)$$

for $j = 0, 1$, with

$$H_0(v_{\parallel}, v_{\perp}) = \frac{1}{2} \left(\frac{k_{\parallel}w_{\perp}^2}{\omega} \right) \frac{\partial f}{\partial v_{\parallel}} - \left(1 - \frac{k_{\parallel}v_{\parallel}}{\omega} \right) f_0(v_{\parallel}, v_{\perp}), \quad (12)$$

$$H_1(v_{\parallel}, v_{\perp}) = \frac{1}{2} \left(\frac{k_{\parallel}w_{\perp}^2}{\omega} \right) \frac{\partial f}{\partial v_{\parallel}} \frac{v_{\perp}^4}{w_{\perp}^4} - \left(1 - \frac{k_{\parallel}v_{\parallel}}{\omega} \right) f_0(v_{\parallel}, v_{\perp}) \frac{v_{\perp}^2}{w_{\perp}^2}. \quad (13)$$

III. NUMERICAL EVALUATION OF χ

The perpendicular velocity integrals produce smoothly varying functions of v_{\parallel} whose product with the singular function $S = (\omega - k_{\parallel}v_{\parallel} - n\Omega)^{-1}$ must then be integrated in v_{\parallel} . For a non-drifting Maxwellian parallel-velocity distribution function with thermal velocity v_{th} , these integrals can be represented in terms of the plasma dispersion function $Z(\zeta/v_{th})$ [12] where $\zeta = (\omega - n\Omega)/k_{\parallel}$. For more general distributions, the integrations must be done numerically. Since these integrals are computed numerous times in forming the matrix system of field equations, efficient evaluation is essential. Further, since the co-factor of S is smooth, the resultant parallel integral's dependence on ζ will be smooth as well. We use this observation by evaluating the integrals at uniformly spaced points ζ_k and then interpolating the results to the desired value of ζ . Efficiency is gained by specifying the distribution function, and thus the co-factors, on the same, uniform, parallel velocity mesh, $v_k = k \Delta v$. Specifically, at a mesh point k , the integrals are of the form

$$I_k = \int dv \frac{C(v)}{v - v_k}. \quad (14)$$

We approximate the cofactors

$$C(v) = \sum_j c_j T_j, \quad (15)$$

where $c_j = C(v_j)$ and where T_j a linear tent function surrounding v_j

$$T_j = \begin{cases} 1 - \frac{|v-v_j|}{\Delta v} & \text{if } |v - v_j| \leq \Delta v, \\ 0 & \text{otherwise.} \end{cases} \quad (16)$$

Then

$$I_k = \sum_j \int dv \frac{f_j T_j}{v - v_k} = \sum_j f_j K_{j-k} = \sum f_{j+k} K_j. \quad (17)$$

where the kernel

$$K_j = \int_{-1}^1 dv \frac{1 - |v|}{v + j\Delta v} = \begin{cases} \ln\left(\frac{j+1}{j-1}\right) - j \ln\left(\frac{j^2}{j^2-1}\right) & |j| > 1, \\ \pm \ln 4 & j = \pm 1, \\ i\pi & j = 0. \end{cases} \quad (18)$$

The convolutions incur modest computational cost. For example, for a parallel velocity grid containing 200 points, the evaluation of the required hot plasma dielectric elements takes about 4 times as long as for evaluation based on analytic approximations (power series and

asymptotic expansion, as appropriate) to Z . The total run time is about twice as long. The dielectric computation time scales as the problem size (number of mesh points) squared, while the matrix solution time scales as the problem size cubed, so, for larger problems, the impact on overall run time is even less than a factor of two.

IV. APPLICATIONS

A. Parameters

To validate the algorithm, calculations are presented of minority hydrogen heating in a plasma equilibrium constructed from Alcator C-Mod tokamak[13] data, shot number 1051206002 at 1120 msec. The poloidal magnetic field configuration is shown in Fig. 1. The electron and (common) ion temperature profiles, taken in a radial cut through the magnetic axis are shown in Fig. 2a. The corresponding electron density profile is shown in Fig. 2b. The profiles are analytic, of the form $(1 - \psi^a)^b$, where $a = 1.5$, (resp. 1.9) and $b = 1.1$ (resp. 1.9) for density and all temperatures, respectively, and where the normalized ψ ranges from 0 to 1. The toroidal field at the magnetic axis is 5.3 Tesla. The toroidal plasma current is 627 kA. The safety factor ranges from .95 on axis to 8 at the plasma edge. The plasma edge, and vacuum vessel radii are 21.26 and 31.26 cm respectively. The plasma consists of 8% fractional number density of hydrogen and 92% deuterium. The wave parameters are: frequency $f = 80.5$ MHz and toroidal wavenumber $n_\phi = 10$, which places the fundamental H and second harmonic D resonances at .12 cm radially. The ion-ion hybrid resonance and cutoffs are at -4 and -2.7 cm, respectively.

B. Isotropic Maxwellian Distributions

The reference calculation is that for isotropic Maxwellian distributions, using the Z function to evaluate χ . Several qualitative features are clearly visible in the surface plot of $\Re E^-$, where $E^- \equiv E_x - iE_y$ (in Stix coordinates) shown in Fig. 3. The long wavelength fast wave, launched from the low-field side midplane at 27.26 cm is converted near the magnetic axis into a combination of moderate wavelength ion cyclotron waves (ICW, emanating rightward, toward the low field side) and short wavelength ion Bernstein waves (IBW, emanating leftward, toward the high field side). The relative power absorbed by second harmonic D,

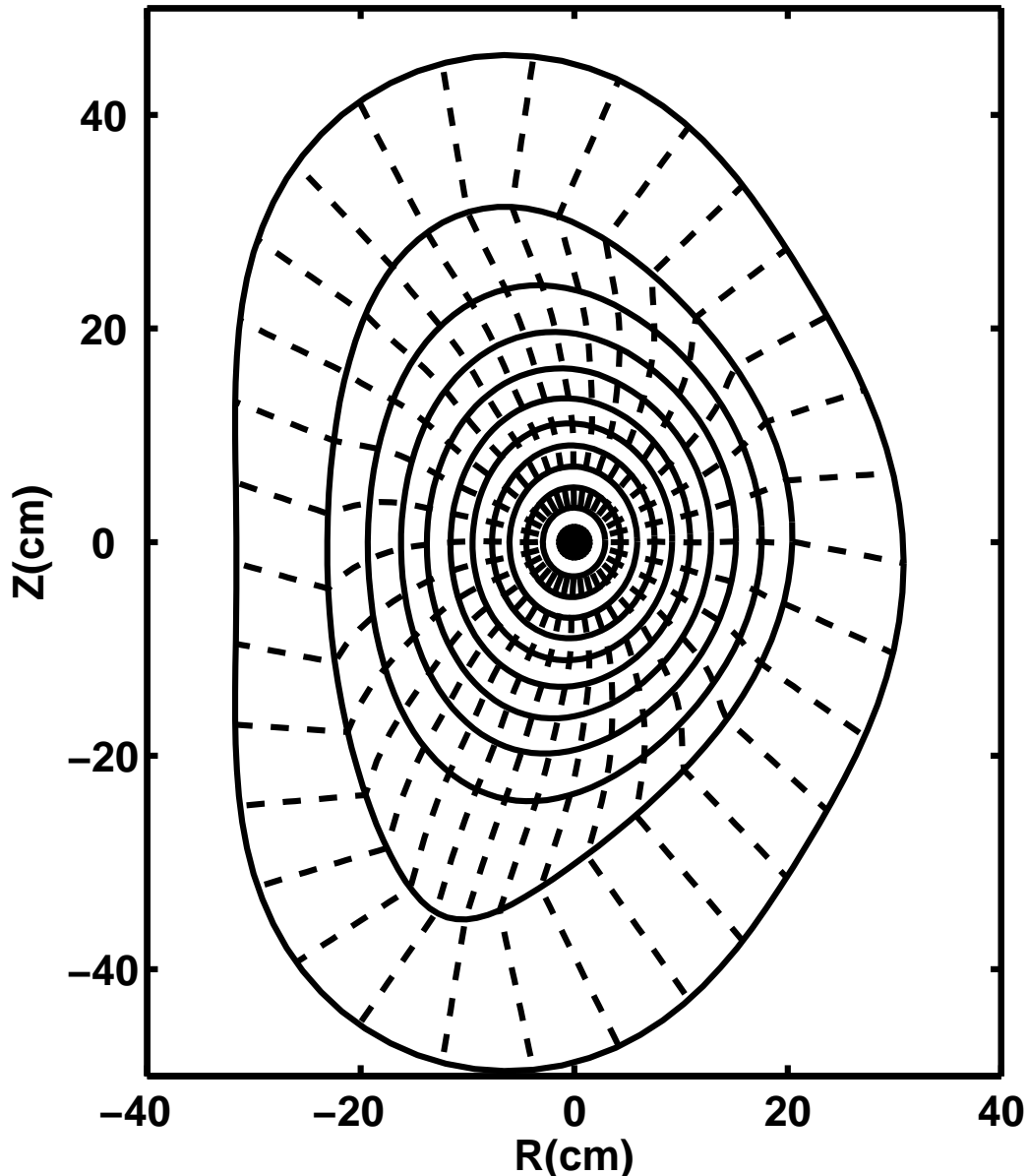


FIG. 1: C-Mod magnetic field geometry – cross section at constant toroidal angle. Shown are a subset of 10 equally spaced (solid) lines of constant poloidal flux ψ , and 32 (dashed) lines of constant TORIC poloidal coordinate angle θ . The full computational mesh has size $n_\psi = 480$, $n_\theta = 256$.

fundamental H and by the electrons for each wave branch is presented in Table I in the column labeled “Reference.” To check the accuracy of the method, the results were re-computed with the minority H susceptibility calculated numerically as described in Section III for a Maxwellian distribution prescribed on a uniform numerical mesh of “low” (column Num-

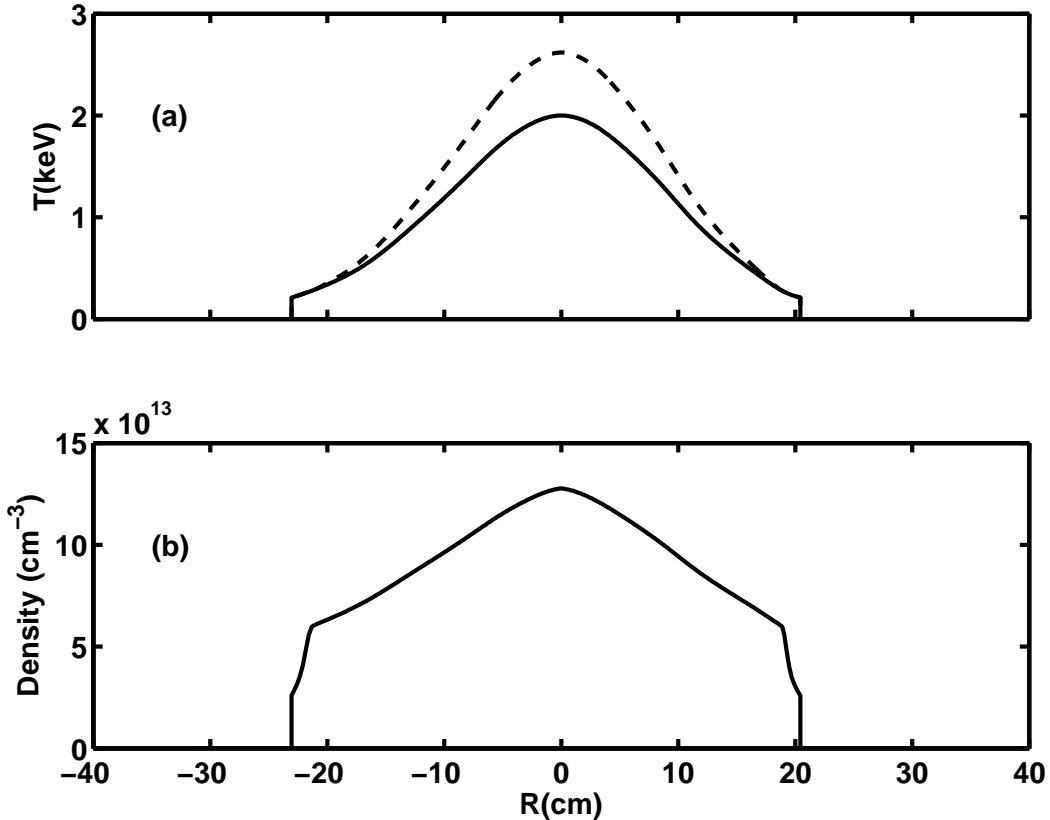


FIG. 2: Profile of electron (dashed) and ion (solid) temperature (a) and electron density (b), taken in a radial cut through the magnetic axis

L) resolution, $N_{\parallel} = 200$ points, $N_{\perp} = 50$ points, and relatively higher resolution (column Num-H), $N_{\parallel} = 800$, $N_{\perp} = 100$. In both cases, the mesh range is $-8v_{th} \leq v_{\parallel} \leq 8v_{th}$, $0 \leq v_{\perp} \leq 10v_{th}$. The power flow channels are well converged to the reference case for both resolutions. A more discriminating measure of convergence is shown in Fig. 4. There the differences $\Re \Delta E^{-} = \Re(E_{\text{numeric}}^{-} - E_{\text{reference}}^{-})$, taken along the line of constant θ , shown in Fig. 3, are plotted for the “low” (4a) and “higher” (4b) resolution simulations, together with field from the reference calculation (4c).

C. Anisotropic Maxwellian Ion Distributions

The sensitivity of the principal absorption channel at the fundamental hydrogen resonance to changes in the shape of the hydrogen distribution was investigated by performing two

Absorbed fraction	Reference	Num-H	Num-L
2 nd Harmonic D	12.9	13.0	12.9
Fundamental H	80.5	80.2	79.7
Electrons - FW	4.61	4.77	5.30
Electrons - IBW	2.01	2.04	2.08

TABLE I: Power flow to each Maxwellian species. The reference simulation evaluates χ , using either a power series or an asymptotic representation of the plasma dispersion function for moderate and large arguments, respectively. Num-H and Num-L designate simulations with numerically computed minority H susceptibility χ_H at higher (Num-H) and at lower (Num-L) parallel velocity resolution in the representation of the distribution function.

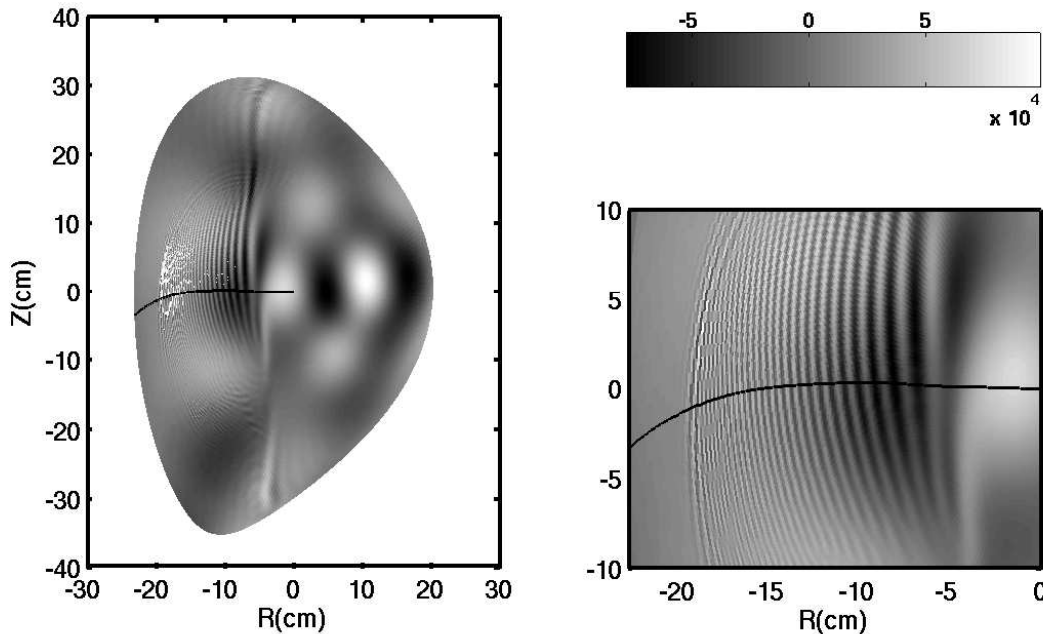


FIG. 3: Surface plot of $\Re E^-$ polarization of wave electric field from the reference computation where all susceptibilities are evaluated using the plasma dispersion function Z . Full plasma cross section (left) and magnified view (right) of region surrounding the line of constant θ , extending leftward from the vicinity of the magnetic axis $(0,0)$, used below to examine convergence of field variation with increasing parallel velocity resolution. Field amplitude is in units of Volts/meter at 1 MW incident power.

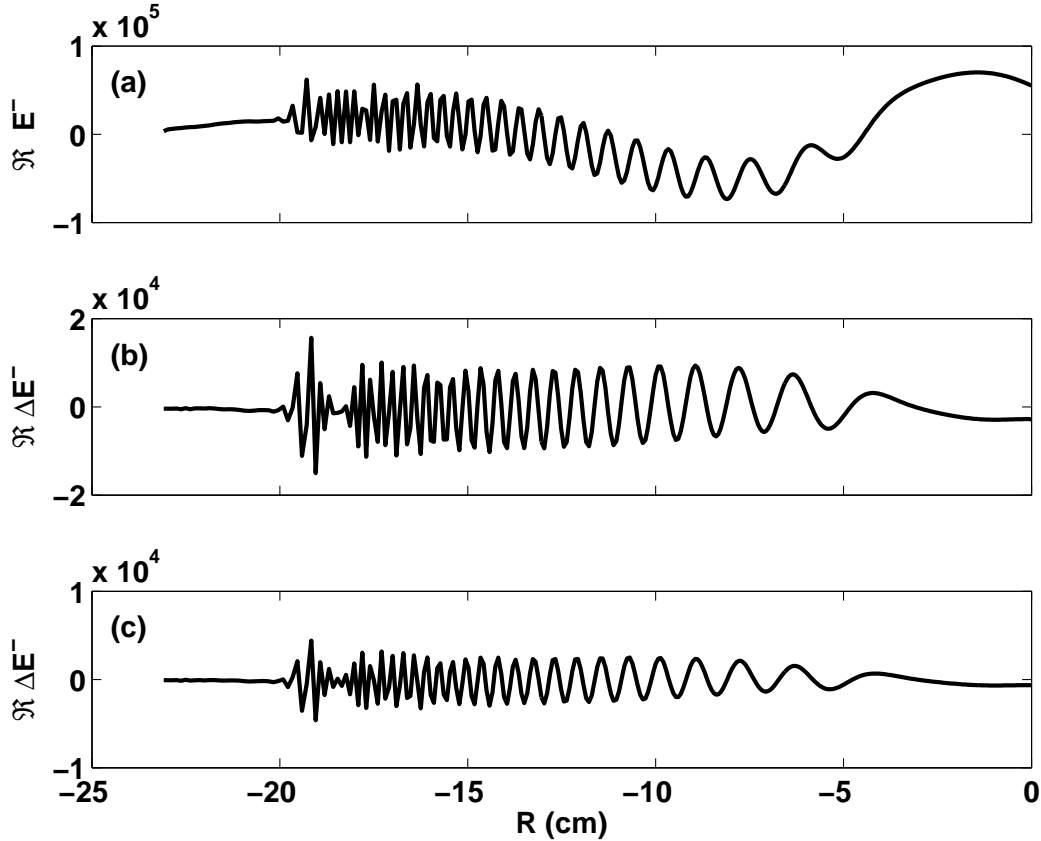


FIG. 4: Variation of $\Re E_{\text{ref}}^-$ (solid) along the constant θ line plotted in red in Fig. 3, together with the difference between the fields computed with low (dot) and high (dash) resolution numerical representations of the minority H distribution and the reference field, along the same line.

series of computations, assuming an anisotropic Maxwellian form for the H distribution

$$f_H(v_{\parallel}, v_{\perp}) = (2\pi)^{-3/2} (v_{th,\parallel} v_{th,\perp}^2)^{-1} \exp[-(v_{\parallel}/v_{th,\parallel})^2 - (v_{\perp}/v_{th,\perp})^2] \quad (19)$$

with $v_{th,\parallel} = \sqrt{(2C_{\parallel}T(\psi)/m_H)}$, $v_{th,\perp} = \sqrt{2C_{\perp}T(\psi)/m_H}$, with constants C_{\parallel} and C_{\perp} parameterizing the scans. The fundamental H absorption fraction, $P_{H,0}$ varied by less than one percent when C_{\perp} was varied from .5 to 10, with C_{\parallel} held fixed at unity. In contrast the second series, in which C_{\perp} was fixed at unity and C_{\parallel} was varied showed a significant variation. For $C_{\parallel} = \{.5, 1., 2., 5., 10.\}$, the corresponding $P_{H,0} = \{71.7, 79.8, 86.9, 93.4, 96.3\}$. In addition, while the absorption profile is localized to the resonant layer for small C_{\parallel} it is significantly broadened radially at for large C_{\parallel} . This is clearly demonstrated in Fig. 5 where the absorption vs (R, Z) is shown for the extreme cases $C_{\parallel} = .5$ (a) and $C_{\parallel} = 10$. (b).

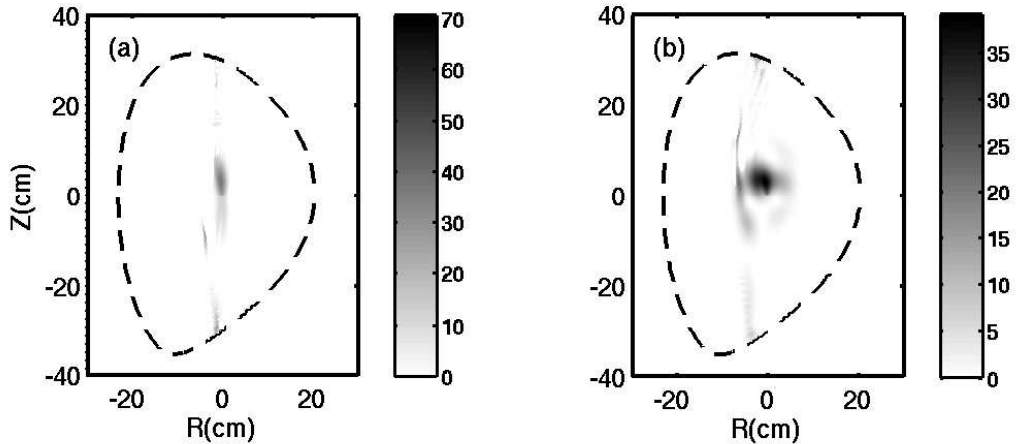


FIG. 5: Surface plots of fundamental absorption by minority Hydrogen for (a) $C_{\parallel} = .5$ and (b) $C_{\parallel} = 10$. The dotted curves delineate the plasma boundary. Units are Watts/cm³ at 1MW incident power.

V. DISCUSSION

The ICRF wave simulation code TORIC has been generalized to allow prescription of arbitrary particle distribution functions of the form $f(v_{\parallel}, v_{\perp}, \theta, \psi)$ in the computation of the plasma susceptibility at modest additional computational cost. The algorithm was validated by recovering results for minority H heating in Alcator CMOD obtained by computing χ using analytic approximations to the plasma dispersion function for the case when all species are Maxwellian. It was shown that, for anisotropic Maxwellian minority H, the power flow at the H fundamental is insensitive to variations in perpendicular temperature, but varies directly with changes in parallel temperature.

-
- [1] T. H. Stix. Fast-wave heating of a two-component plasma. *Nucl. Fusion*, 15:737, 1975.
- [2] M. Brambilla. Numerical simulation of ion cyclotron waves in tokamak plasmas. *Plasma Phys. Controlled Fusion*, 41:1, 1999.
- [3] D. N. Smithe. Local full-wave energy and quasilinear analysis in nonuniform plasmas. *Plasma Phys. Controlled Fusion*, 31:1105, 1989.
- [4] R. J. Dumont, C. K. Philips, and D. N. Smith. Effects of non-maxwellian species on ion cyclotron waves propagation and absorption in magnetically confined plasmas. *Phys. Plasma*, 12:042508, 2005.
- [5] E. F. Jaeger *etal.* All-order spectral calculation of radio-frequency heating in two-dimensional toroidal plasmas. *Phys. Plasma*, 8:1573, 2001.
- [6] E. F. Jaeger *etal.* Sheared poloidal flow driven by mode conversion in tokamak plasmas. *Phys. Rev. Lett.*, 90:195001, 2003.
- [7] R. W. Harvey and M. G. McCoy. In *Proceedings of the IAEA Technical Committee Meeting on Simulation and Modeling of Thermonuclear Plasma, Montreal, Canada, 1992*. Available as USDOC NTIS Document No. DE93002962.
- [8] E. F. Jaeger *etal.* Self-consistent full-wave and fokker-planck calculations for ion cyclotron heating in non-maxwellian plasmas. *Phys. Plasma*, 13:056101, 2006.
- [9] M. Brambilla. Electron landau damping of ion bernstein waves in tokamak plasmas. *Nucl. Fusion*, 38:1805, 1998.
- [10] T. H. Stix. *Waves in Plasmas*. American Institute of Physics, 1992.
- [11] R. J. Dumont C. K. Phillips, A. Pletzer and D. N. Smith. Plasma dielectric tensor for non-maxwellian distributions in the fir limit. In *Radio Frequency Power in Plasmas, Proceedings of the 15th Topical Conference on Radio Frequency Power in Plasmas*, page 499. AIP, NY, May 19-21 2003.
- [12] B. D. Fried and S. D. Conte. *The Plasma Dispersion Function*. Academic Press, NY, 1961.
- [13] P. T. Bonoli *etal.* newblock Mode converison electron heating in Alcator C-Mod: Theory and experiment. *Phys. Plasma*, 7:1886, 1999.

The Princeton Plasma Physics Laboratory is operated
by Princeton University under contract
with the U.S. Department of Energy.

Information Services
Princeton Plasma Physics Laboratory
P.O. Box 451
Princeton, NJ 08543

Phone: 609-243-2750
Fax: 609-243-2751
e-mail: pppl_info@pppl.gov
Internet Address: <http://www.pppl.gov>